Parametrizations of size distribution and refractive index of biomass burning organic aerosol with black carbon content

Biao Luo[1,2], Ye Kuang[1,2,*], Shan Huang[1,2*], Qicong Song[1,2], Weiwei Hu[3], Wei Li[1,2], Yuwen Peng[1,2], Duohong Chen[4], Dingli Yue[4], Bin Yuan[1,2], Min Shao[1,2]

[1] Institute for Environmental and Climate Research, Jinan University, Guangzhou, China.

[2] Guangdong-Hongkong-Macau Joint Laboratory of Collaborative Innovation for Environmental Quality, Guangzhou, China.

[3] State Key Laboratory of Organic Geochemistry and Guangdong Key Laboratory of Environmental Protection and Resources Utilization, Guangzhou Institute of Geochemistry, Chinese Academy of Sciences, Guangzhou 510640, China

[4] Guangdong Ecological and Environmental Monitoring Center, State Environmental Protection Key Laboratory of Regional Air Quality Monitoring, Guangzhou 510308, China

Corresponding author: Ye Kuang (kuangye@jnu.edu.cn) and Shan Huang (shanhuang_eci@jnu.edu.cn)

Abstract

Biomass burning organic aerosol (BBOA) impacts significantly on climate directly through scattering and absorbing solar radiation and indirectly through acting as cloud condensation nuclei. However, fundamental parameters in the simulation of BBOA radiative effects and cloud activities such as size distribution and refractive index remain poorly parameterized in models. In this study, biomass burning events with high combustion efficiency characterized by high black carbon (BC) to BBOA ratio (0.22 on average) were frequently observed during autumn in the Pearl River Delta region, China. An improved absorption Ångström exponent (AAE) ratio method considering both variations and spectral dependence of black carbon AAE was proposed to differentiate brown carbon (BrC) absorptions from total aerosol absorptions. BBOA size distributions, mass scattering and absorption efficiency were retrieved based on the changes in aerosol number size distribution, scattering coefficients and derived BrC absorptions that occurred with BBOA spikes. Geometric mean diameter of BBOA volume size distribution D_{gv} depended largely on combustion conditions, ranging from 245 to 505 nm, and a linear relationship between D_{gv} and $\Delta BC/\Delta BBOA$ was achieved. Retrieved real part of BBOA refractive index ranges from 1.47 to 1.64, with evidences showing that its variations might depend largely on combustion efficiency, which is rarely investigated in existing literatures however requires further comprehensive investigations. Retrieved imaginary parts of BBOA refractive index ($m_{i,BBOA}$) correlated highly with $\Delta BC/\Delta BBOA$ ($R>0.88$) but differ much with previous parameterization schemes. The reason behind the inconsistency might be that single formula parameterizations of $m_{i,BBOA}$ over the whole BC/BBOA range were used in previous studies which might deviate substantially for specific BC/BBOA ranges. Thus, a new scheme that parameterize wavelength-dependent $m_{i,BBOA}$ was presented, which filled the gap for field-based BBOA absorptivity paramterizations of BC/BBOA>0.1. These findings have significant implications for simulating BBOA climate effects and suggest that linking both BBOA refractive index and BBOA volume size dsitrbutions to BC content might be a feasible and a good choice for climate models.

1 Introduction

Biomass burning organic aerosol (BBOA) emitted from natural and anthropogenic fire activities, represents a major fraction of atmospheric primary organic aerosols, impacts significantly on climate and regional air quality directly through scattering and absorbing solar radiation and indirectly through acting as cloud condensation nuclei (Saleh et al., 2014;Saleh et al., 2015;Wang et al., 2016a;Zhang et al., 2020;Liu et al., 2020b). BBOA size distributions are crucial for simulating aerosol-cloud interactions, and BBOA scattering play significant role in direct aerosol cooling effects and local visibility degradation. BBOA is also a major contributor to atmospheric brown carbon (BrC) on a global scale (Wang et al., 2016a) because of its non-negligible light absorption contribution in the near-ultraviolet to visible wavelength. Accurate representation of BBOA size distributions, scattering and absorption in climate models are crucial for BBOA radiative forcing simulations, and bias in biomass burning absorption representation in models can result in biomass burning radiative forcing range from cooling to warming (Brown et al., 2021). BBOA size distribution and refractive index are fundamental parameters in the simulation of BBOA radiative effects and cloud activities, however, remain poorly parameterized in models. Currently, our comprehensive knowledge of BBOA optical and physical properties were primarily obtained from laboratory measurements (Janhäll et al., 2010;Saleh et al., 2013;McClure et al., 2020). Although field measurements of biomass burning events were reported by many studies (Laskin et al., 2015), however, only a few of them focused simultaneously on both BBOA size distributions and optical properties (Reid et al., 2005b;Reid et al., 2005a;Laing et al., 2016), and their parameterizations were reported by few studies. Comprehensive field measurements and simultaneous characterization of BBOA size distributions, scattering and absorption properties and retrieval of real and imaginary part of BBOA refractive index as well as their parameterizations remain lacking, hindering the accurate representation of BBOA size distributions and refractive index in climate models.

In-situ field measured aerosols are mixtures of different aerosol components emitted from different sources and formed through different pathways. The BBOA mass concentrations might be identified through source apportionment of organic aerosols using positive matrix factorization (PMF) technique on the basis of aerosol mass spectrometer measurements (Kuang et al., 2021). However, the BBOA size distributions, BBOA scattering properties and BBOA light absorptions are usually quite

difficult to separate from properties of the entire aerosol populations. As a result, BBOA physical properties such as size distribution, mass scattering efficiency (MSE), mass absorption efficiency (MAE) and refractive index of biomass burning aerosols characterized in in-situ field measurements are usually not specific to BBOA (Laing et al., 2016). Especially, parameterization of the imaginary part of the BBOA refractive index ($m_{i,BBOA}$) have received wide attentions in recent years due to its critical role in BBOA absorptivity representation in climate models (Saleh, 2020). However, the yet available parameterization schemes were primarily based on laboratory experiments, with very few field measurements based results available (Lu et al., 2015). Liu et al. (2021) observed the evolution of $m_{i,BBOA}$ in a real atmospheric environment chamber for different fire conditions at hourly scales after emission under different oxidation conditions. Still, the spectral dependence parameterization of $m_{i,BBOA}$ on the basis of in-situ field measurements covering a wavelength range from ultraviolet to near-infrared remain lacking.

The key reason limiting the on-line characterization of BBOA refractive index based on the real atmosphere measurements is that the on-line accurate quantification of BrC light absorption has been a challenge due to the entanglement of black carbon (BC) absorption. Many studies have shown that the distinct difference between BC and BrC spectral absorption characteristics represented by Ångström law can be used to segregate BrC absorptions from measured total aerosol absorptions by assuming a constant absorption Ångström exponent (AAE) of BC (AAE_{BC}) (de Sa et al., 2019;Wang et al., 2016b;Yang et al., 2009). The BrC absorption retrieval accuracy of this constant AAE method depends highly on the representativeness of used AAE_{BC}. Results of field and laboratory studies demonstrated that AAE_{BC} varies under different pollution and emission conditions (Zhang et al., 2019a;Laskin et al., 2015). Model simulations and field observations show that AAE_{BC} is affected by many factors such as BC mixing state, morphology, BC mass size distribution as well as optical wavelength, and values of AAE_{BC} can reach up to 1.6 for specific wavelength pairs (Lack and Cappa, 2010). Recent studies have modified the AAE method through a better consideration of AAE_{BC} variations. Zhang et al. (2019b) used the $AAE_{880\text{-}990}$ obtained from real-time aethalometer measurements as AAE_{BC}, considering that aerosol absorptions at near infrared wavelengths are associated only with BC. Other studies determined AAE_{BC} through Mie theory simulations using constrained BC mass or BC mixing states as inputs (Li et al., 2019;Wang et al., 2018;Qin et al., 2018;Wang et al., 2016b). Wang et al. (2018) found remarkable AAE_{BC} wavelength dependence and a

relatively stable ratio between AAE_{BC} of certain wavelength ranges, which could be used to represent spectral dependence of AAE_{BC}. However, this ratio method proposed by Wang et al. (2018) assumes that BrC absorption contributes negligibly at 520 nm, which might bring some uncertainties and cannot be used to retrieve the spectral characterization of BrC absorption for wavelengths near and beyond 520 nm.

In this study, aerosol chemical compositions, size distributions as well as aerosol scattering and absorption coefficients were measured at a rural site in the Pearl River Delta (PRD) region of China, where biomass burning events frequently occurred in autumn and played significant roles in regional air quality (Liu et al., 2014). An improved method considering both variations and spectral dependence of AAE_{BC} was proposed to quantify the BrC absorption spectral dependence from 370 nm to 660 nm. The differential method was applied to biomass burning events to estimate BBOA scattering and absorption properties as well as BBOA size distributions. The combination of identified BBOA size distributions, MSE and MAE were used to retrieve the real and imaginary parts of BBOA refractive index using the Mie theory, based on which parameterizations of BBOA size distributions and refractive index using BC/BBOA ratio were investigated.

2 Materials and methods

2.1 Field measurements.

Field measurements were performed from 30 September to 17 November 2019 at a rural site in Heshan county, Guangdong Province, China. The site locates at the top of a small hill surrounded by small villages and residential towns, and usually experiences air masses from cities of the highly industrialized PRD region. This site is authorized as a supersite operated by the provincial environmental monitoring authority, therefore continuous qualified measurements of meteorological parameters such as air temperature, relative humidity (RH), wind speed and direction, and pollutant measurements such as carbon monoxide, ozone and nitrogen oxides are carried out. Physical and chemical properties of ambient aerosol were comprehensively measured during this field campaign, including multi-wavelength (450 nm, 525 nm, 635 nm) aerosol scattering coefficients (nephelometer, Aurora 3000) measurement under nearly dry (RH<30%) and controlled but fixed RH conditions using humified nephelometer system (Kuang et al., 2020), multi-wavelength absorption measurements using an aethalometer (Magee, AE33 (Drinovec et al., 2015b)), aerosol size distribution measurements using

a scanning mobility particle sizer (SMPS, TSI 3080) and an aerodynamic particle sizer (APS; TSI Inc., Model 3321), and aerosol chemical composition measurements using an soot-particle aerosol mass spectrometer, etc. The AE33 measurements were only valid from 30 September to 31 October. Continuous and stable measurements of aerosol chemical composition using the aerosol mass spectrometer measurements were valid since 10 October. More details on the site and instrument set up can be found in (Kuang et al., 2021).

Accurate AAE and absorption measurements are crucial for the BrC quantification. Results of previous comparison studies of aerosol absorption measurements between AE33 and photoacoustic soot spectrometer demonstrated that AAE will only be slightly influenced by the particle collection of AE33 on the filter (Saleh et al., 2013;Zhao et al., 2020). However, aerosol absorption values measured by AE33 bear uncertainties associated with loading and multiple scattering effects. Dual-spot mode was applied in AE33 measurements for dealing with aethalometer loading effect. A Multiple-scattering correction factor (C) was used to convert measured attenuation coefficient (b_{ATN}) by AE33 to the absorption coefficient of ambient aerosols (b_{abs}) at each wavelength through $b_{abs} = b_{ATN}/C$. C is considered to be dependent on filter tape (Drinovec et al., 2015a) and aerosol chemical compositions (Wu et al., 2009;Collaud Coen et al., 2010). Results of Yus-Díez et al. (2021) showed that C values increased considerably when single scattering albedo (SSA) is higher than 0.95. However, as shown in Fig.S5, SSA is much lower than 0.95 during this field campaign with an average of 0.78. Moreover, the filter tape 8060 was used for AE33 during this field campaign. Zhao et al. (2020) evaluated C of filter tape 8060 through comparing AE33 measurements with a three-wavelength photoacoustic soot spectrometer, and their results demonstrated that C is almost independent of wavelength and differs little among measurements of different locations. Thus the wavelength independent C of filter tape 8060 of 2.9 recommended by Zhao et al. (2020) was used, and this value is also almost the median value of C ranges used in Kasthuriarachchi et al. (2020).

2.2 Aerosol mass spectrometer measurements.

The size-resolved aerosol chemical compositions of dried aerosol particles with aerodynamic diameter less than 1 μm were measured using a soot particle aerosol mass spectrometer (SP-AMS, Aerodyne Research, Inc., Billerica, MA, USA). As discussed in Kuang et al. (2021), the mass concentrations of aerosol chemical compositions from SP-AMS were validated by offline $PM_{2.5}$ filter

measurements, SMPS aerosol volume concentration measurements and online measurements for inorganic aerosol components. The source identification of organic aerosols was conducted using PMF method based on the high-resolution OA data collected in V-mode (only tungsten vaporizer). As introduced in Sect.S1, six OA factors were identified based on the best performance criteria of PMF quality parameters, more details about the determination factor number and factor sources are presented in Sect.S1. Two primary OA factors include BBOA (O/C=0.48) and a hydrocarbon-like organic aerosols (HOA, containing cooking emissions, O/C=0.02). The other four factors were associated with secondary formations or aging processes: 1) more oxygenated organic aerosols (MOOA, O/C=1, associated with regional airmass (Kuang et al., 2021)), 2) less oxygenated organic aerosols (LOOA, O/C=0.72, related to daytime photochemical formation), 3) nighttime-formed organic aerosols (Night-OA, O/C=0.32, highly correlated with Nitrate with r=0.67, and exhibited sharp increases during the evening), and 4) aged BBOA (aBBOA, O/C=0.39, exhibited similar diurnal behavior with LOOA with strong daytime production). The mass spectral profile and time series of these organic aerosol factors were shown in Fig.S2, and details about the determination of these factors are introduced in Sect .S1. The BBOA factor will be the focus of this study. On the basis of the scheme proposed by Kuwata et al. (2012), the density of BBOA (ρ_{BBOA}) and HOA was estimated as 1.25 and 1.15 g/cm^3 with O:C and H:C as inputs, and used in this study.

2.3 Quantification of BrC absorptions based on the light absorption wavelength dependence measurements.

BrC absorbs significantly at near-UV and short-visible wavelengths but exhibits strong wavelength dependence (Saleh, 2020). The deconvolution of the spectral dependence of measured aerosol light absorption has been a common method to retrieve the BrC and black carbon (BC) absorption distribution:

$$\sigma_{BrC}(\lambda) = \sigma_a(\lambda) - \sigma_{BC}(\lambda) \quad (1)$$

Where $\sigma_a(\lambda)$ represents measured total aerosol absorption at wavelength λ, $\sigma_{BC}(\lambda)$ the absorption associated with BC (includes influences of BC size distributions and mixing states, etc.), and $\sigma_{Brc}(\lambda)$ the light absorption contributed by BrC. The spectral dependence of BC absorption was usually accounted for using the Ångström exponent law (Laskin et al., 2015), which describes BC absorption as $\sigma_{BC}(\lambda) = K\lambda^{-AAE}$ where K is a constant factor associated with BC mass concentration. The

traditional method usually assumes a constant AAE_{BC} of 1(de Sa et al., 2019) , or a wavelength independent AAE_{BC} derived from near infrared absorption measurements by assuming that the BrC absorption is negligible at near infrared wavelengths. For example, $\sigma_{BC}(880\ nm)$ and $\sigma_{BC}(950\ nm)$ measured by AE33 can be used to formulate the spectral dependence of aerosol absorptions associated with BC as the following:

$$\sigma_{BC}(\lambda) = \sigma_{BC}(880\ nm) \times (\frac{880}{\lambda})^{AAE_{BC,\lambda-880}} \quad (2)$$

$$AAE_{BC,\lambda-880} = AAE_{BC,950-880} \quad (3)$$

However, several recent modelling studies using Mie-theory and BC measurements demonstrated that AAE_{BC} varies as a function of wavelength, and the wavelength independent assumption of AAE_{BC} will bring large uncertainties into BrC calculation (Li et al., 2019;Wang et al., 2018). Wang et al. (2018) found $AAE_{BC,520-880}$ and $AAE_{BC,370-520}$ differed much from each other, however, the $AAE_{BC,370-520}/AAE_{BC,520-880}$ ratio varied little, and thus proposed an AAE ratio method to obtain real-time $AAE_{BC,370-520}$ and further deduced $\sigma_{BC}(370\ nm)$. This method assumes that BrC contributes negligibly at 520 nm, which might introduce uncertainties. In addition, this method is not applicable in retrieving the spectral dependence of BrC absorption because only the ratio $AAE_{BC,370-520}/AAE_{BC,520-880}$ was used. This modified wavelength-dependent AAE differentiation method was further partially adopted by Li et al. (2019), using $AAE_{BC,370-520}$ to account for spectral dependence of BC absorption for wavelengths<520 nm and $AAE_{BC,520-880}$ for wavelengths>520 nm, thus the wavelength-dependent AAE_{BC} was partially but not thoroughly considered.

In this study, we introduce a AAE ratio $R_{AAE}(\lambda)=AAE_{BC,\lambda-880}/AAE_{BC,950-880}$ to take spectral dependence of AAE_{BC} into account and use on-line measurements of $AAE_{950-880}$ as $AAE_{BC,950-880}$ under the assumption of that negligible absorption contributions of BrC at wavelengths of 880 nm and 950 nm. Thus, absorption measurements of 370 nm, 470 nm, 530 nm, 590 nm and 660 nm can be used to retrieved the spectral dependence of BrC absorptions.

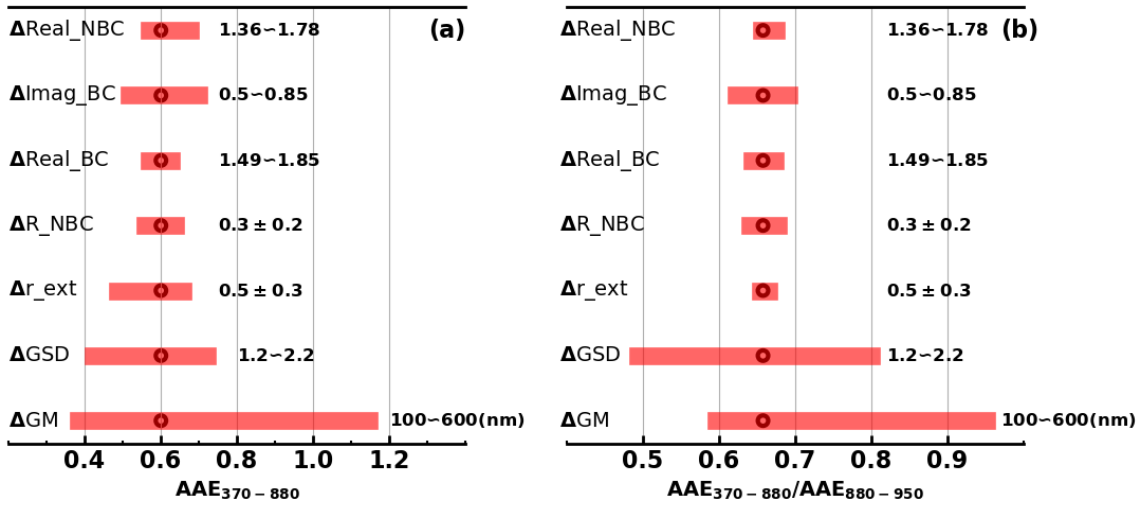

Figure 1. Changes in (a) $AAE_{BC,370-880}$ and (b) $AAE_{BC,370-880}/AAE_{BC,950-880}$ associated perturbations of different parameters, perturbation ranges of parameters are shown in the right side of the bar.

$R_{AAE}(\lambda)$ are influenced by many factors such as BC refractive index, coating shell refractive index as well as BC mixing state, and BC mass size distributions (Li et al., 2019). A sensitivity experiment following the method of Li et al. (2019) is initiated to explore impacts of these optical and mixing state parameters on $AAE_{BC,\lambda-880}$ and $R_{AAE}(\lambda)$, more details are available in Supplement Sect.S1. These parameters including the real part of the refractive index of BC coating materials and BC-free particles (Real_NBC), real and imaginary parts of refractive index of the BC core (Real_BC and Imag_BC), the mass fraction of externally mixed BC (r_ext), the number fraction of BC-free particles (R_NBC), geometric standard deviation (GSD) and geometric mean diameter (GM) of BC mass size distributions. Note that the imaginary parts of the refractive index of BC particle coating materials and BC-free particles were not perturbed in these simulations and treated as zero under the assumption of materials other than BC is non-absorbing. In order to separate effects of BC and BrC on $AAE_{\lambda-880}$ changes, this assumption must be made to obtain $AAE_{BC,\lambda-880}$ variations associated only with BC absorption changes. Thus, the defect of this method is that the entangling effects of BrC coating on BC particles in $AAE_{BC,\lambda-880}$ variations are not considered. Impacts of these parameters on $AAE_{BC,370-880}$ and $R_{AAE}(370)$ are investigated through perturb parameters within atmospheric relevant ranges reported in

previous studies (Bond et al., 2013;Tan et al., 2016;Zhao et al., 2019), and ranges of these parameters are listed in Fig.1. The results of $AAE_{BC,370-880}$ is shown in Fig.1a. It shows that variations of both refractive index of BC and coating materials as well as BC mixing states have non-negligible influences on $AAE_{BC,370-880}$, however the BC mass size distributions represented by geometric standard deviation (GSD) and geometric mean diameter (GM) of BC mass size distribution play the most important roles. Nevertheless, for results of $AAE_{BC,\lambda-880}/AAE_{BC,950-880}$ shown in Fig.1b, when fixing the BC mass size distribution, $AAE_{BC,\lambda-880}/AAE_{BC,950-880}$ exhibited much smaller variations, even the refractive index of BC and shell or mixing state varied within atmospherically relevant ranges.

The result of sensitive studies shown in Fig.1b confirmed the applicability of the proposed new AAE ratio method under constrained BC mass size distributions. The elemental carbon fragments (C_x) retrieved from SP-AMS measurements cannot be used to quantify BC mass concentrations due to the lack of calibration parameters, however, its size distributions generally represent the relative contributions of BC mass within different diameter ranges. The real-time measured normalized C_x distributions are therefore used to distribute total BC mass to different diameter bins to calculate $R_{AAE}(\lambda)$, and the average normalized C_x distribution is shown in Fig.S6. The average and standard deviations of $R_{AAE}(370)$, $R_{AAE}(470)$, $R_{AAE}(520)$, $R_{AAE}(590)$ and $R_{AAE}(660)$ are 0.79(±0.044), 0.85(±0.038), 0.88(±0.035), 0.9(±0.035) and 0.93(±0.031) respectively. Based on this method, the spectral dependence of BrC absorption can be derived as the following:

$$\sigma_{BrC}(\lambda) = \sigma_a(\lambda) - \sigma_{BC}(880\ nm) \times \left(\frac{880}{\lambda}\right)^{AAE_{BC,950-880} \times R_{AAE}(\lambda)} \quad (4)$$

Results of previous studies (Saleh, 2020;Yu et al., 2021) demonstrated that non-negligible BrC absorptions at near-infrared range, and results of Hoffer et al. (2017) demonstrated that absorption coefficient of tar balls at 880 nm is more than 10% of that at 470 nm. During this campaign, the average aerosol absorption at 880 nm is 26.7 Mm^{-1}, derived average BrC absorption at 470 nm is 11.5 Mm^{-1}, 10% of BrC absorption at 470 nm accounts for on average 4.2% of aerosol absorption at 880 nm and the realistic BrC contribution at 880 nm is likely lower considering that tar balls represent the most efficient BrC. Thus, the assumption that negligible absorption contributions of BrC at wavelengths of 880 nm and 950 nm when deriving $AAE_{BC,950-880}$ from AE33 measurements holds in most cases when BC dominates. In addition, the key part of our newly proposed method is considering the spectral dependence of AAE_{BC} through the ratio $R_{AAE}(\lambda)$ and $AAE_{BC,950-880}$, however, the accurate

$AAE_{BC,950-880}$ derivations need robust performance of AE33 at both 880 nm and 950 nm, thus quality assurance of these measurements should be warranted before using the $AAE_{BC,950-880}$.

3 Results and discussions

3.1 Dominant contribution of BBOA to BrC absorption

Biomass burning plumes around the observation site were frequently observed during this field campaign at dusk as shown in Fig.S7(a,d) and only sometimes during daytime periods (Fig.S7(b, c)). The average diurnal variations of resolved primary OA factors including both BBOA and HOA are presented in Fig.S8, in which both average diurnal profiles of BBOA and HOA exhibited sharp increases around 18:00 local time (LT), which should be associated with frequently observed biomass burning events and supper cooking in villages and towns near this site. However, diurnal behaviors of BBOA and HOA differ much from about 06:00 LT to 16:00 LT. HOA exhibited continuous decreases during this daytime period, which was associated with boundary layer processes and re-partitioning due to increasing temperature. The BBOA showed almost continuous but slow increases since morning to the afternoon, indicating strong daytime emissions of BBOA as shown in Fig.S7(b, c), although not as prominent as the BBOA emission just before the fall of nighttime. The probability distribution of the ratio BBOA/HOA is also shown in Fig.S8b, which shows that the ratio BBOA/HOA reached beyond 2 in 57% conditions with an average of 3.3, which demonstrates that biomass burning was a dominant primary aerosol emission source during this field campaign.

The observed AAEs between different wavelengths and 880 nm of total aerosol absorption are shown in Fig.2a, the average values of $AAE_{370-880}$, $AAE_{470-880}$, $AAE_{520-880}$, $AAE_{590-880}$, $AAE_{660-880}$, $AAE_{950-880}$ are 1.17, 1.23, 1.18, 1.15, 1.08, 1.04. The scatter plots of $AAE_{370-880}$ and the ratio BBOA/BC shown in Fig.2b shows that $AAE_{370-880}$ was highly correlated with BBOA/BC (r=0.8), indicating strong influences of BBOA on aerosol absorption wavelength dependence. The BrC absorption at multiple wavelengths are extracted using the improved AAE ratio method introduced in Sect.2, and statistical ranges of BrC absorption as well as their contributions to total aerosol absorption are shown in Fig.2d. Average values of derived σ_{BrC} at 370 nm, 470 nm, 520 nm, 590 nm, 660 nm are 19.1 Mm^{-1}, 11.5 Mm^{-1},6.4 Mm^{-1},3.45 Mm^{-1},1.13 Mm^{-1} and their contributions to total aerosol absorption are 23%, 18%, 12%, 8%, 3% respectively. Similar to some previous studies (Tao et al., 2020;Qin et al., 2018), these results shows that the contributions of BrC to aerosol absorption at wavelengths of less than 590

nm are not negligible. The derived timeseries of $\sigma_{BrC,370}$ are shown in Fig.S9d, depicting BBOA varying quite consistently with $\sigma_{BrC,370}$ and with high correlations (correlation coefficients between σ_{BrC} at 370 nm, 470 nm, 520 nm, 590 nm, 660 nm and BBOA reaching 0.9, 0.83, 0.8, 0.76, 0.69), suggesting that BBOA was the dominant contributor to BrC absorption.

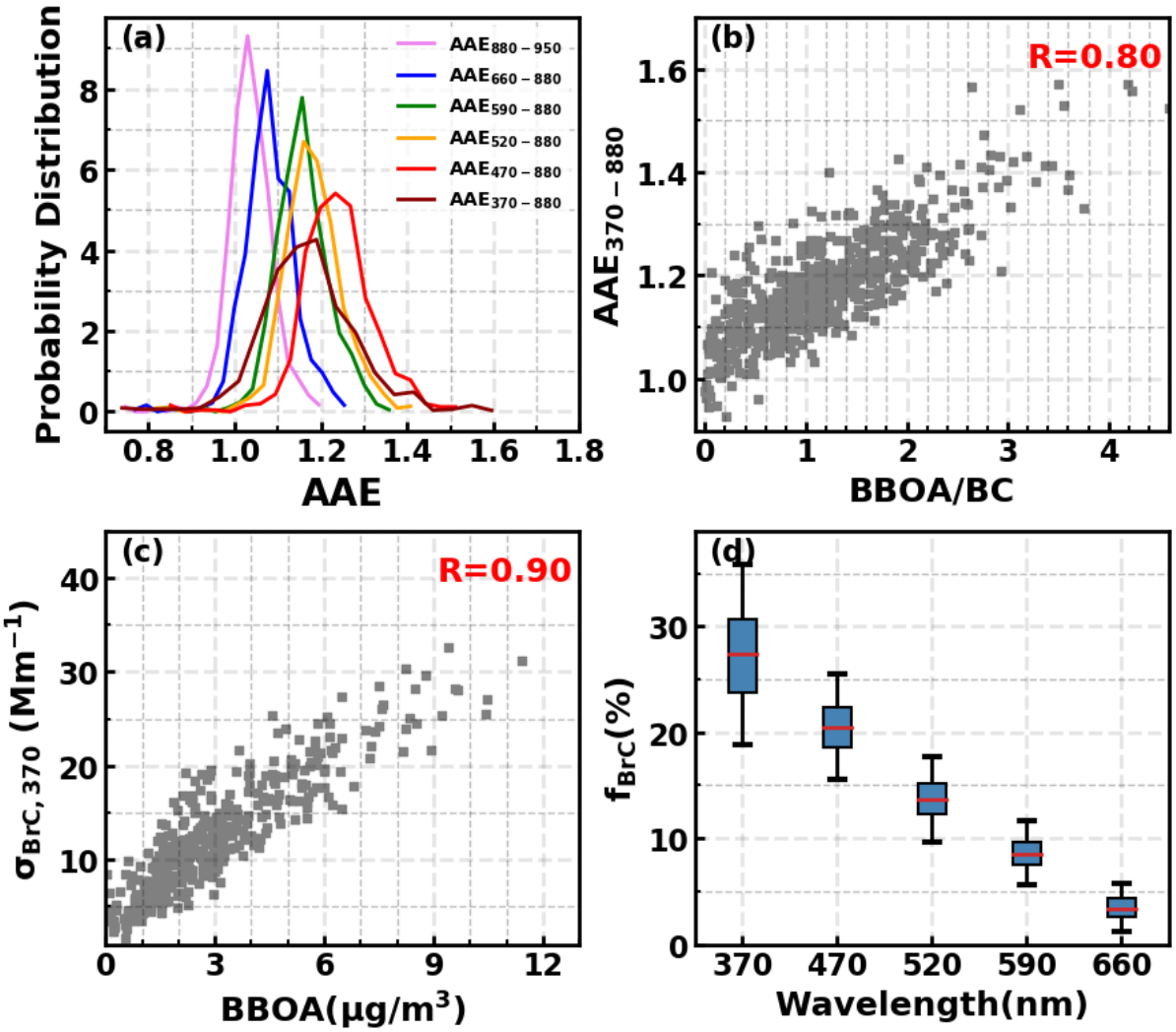

Figure 2. **(a)** Probability distribution of AAE between different wavelengths and 880 nm; **(b)** Correlations between $AAE_{370-880}$ and mass ratio of BBOA and BC; **(c)** Correlations between the BrC absorption coefficients at 370nm and the BBOA mass loadings; **(d)** Box-and-whisker plots of BrC absorption fractions at different wavelengths.

3.2 Identification of BBOA size distributions and their parameterizations

During the observation period, BBOA contributed domominantly to BrC absorptions and notable biomass burning events represented by BBOA mass concentration spikes as shown in Fig.S9

freqeuntly occurred. Events with BBOA increased suddenly, drastically and continuously within half hour to several hours were identified as BBOA spikes. We don't have a criterion on this and we choose spikes artificially, these identified spikes generally last about 0.5-1.5 hours (from the beginning to the peak). The used BBOA spikes were shaded in Fig.S9, some of identified spikes were not used because of the missing of particle number size distribution measurements. These biomass burning spikes are related with biomass burning plumes that swept over the observation site, thus the difference between aerosol properties measured before and during these spikes can represent the properties of biomass burning aerosols. Theses spikes ususally occurred during supper cooking time (~ 18:00 LT) and typical bio-fuels used for cooking are mainly vegetation fuels such as local woods. SMPS directly measures the aerosol paritcle number size distribution (PNSD), thus also providing particle volume size distribution measurements (PVSD). Fig.3a shows the average differences of mass concentrations of different aerosol components of identified sipkes with simultaneous valid SMPS data. Ammonium nitrate (AN) and ammonium sulfate (AS) were determined as the dominant form of ammonium, sulfate and nitrate ions during this field campaign and paired using the scheme paroposed by Gysel et al. (2007). Note that the Δ shown in Fig.3a and also hereafter means the difference between that variable before BBOA increases and when BBOA reach its peak (the definition of the BBOA spike, these peaks are also marked in Fig.S9), corresponding to the start and end of BBOA increase. It shows that inorganic aerosol components increased a little bit, which is consistent with previous studies (Hecobian et al., 2011;Pratt et al., 2011) that biomass burning emitts tiny amounts of inorganic aerosol. However, it is difficult to quantity how much of these inorganic aerosol increases was attributed to biomass burning emissions because the biomass burning spikes were usually observed during the periods with secondary nitrate formation (Kuang et al., 2021). Secondary organic aerosol components changed a little, with the slight increase of aBBOA suggesting plumes were aged a little bit. Obvious increases of HOA were observed, but the most prominent increase was BBOA. The aveage $\Delta BC/\Delta BBOA$ ratio for cases when BC measurements were valid was 0.22, suggesting the observed biomass burning events are likely flaming burning conditions with high combustion efficiency (Reid et al., 2005b;McClure et al., 2020). The cooking related organic aerosol could not be separated from HOA in PMF analysis. The co-increase of HOA are due to the fact that these identifed spikes occured during periods of supper cooking as disccused before.

The average aerosol particle number and volume size distribution differences (Δ PNSD and Δ

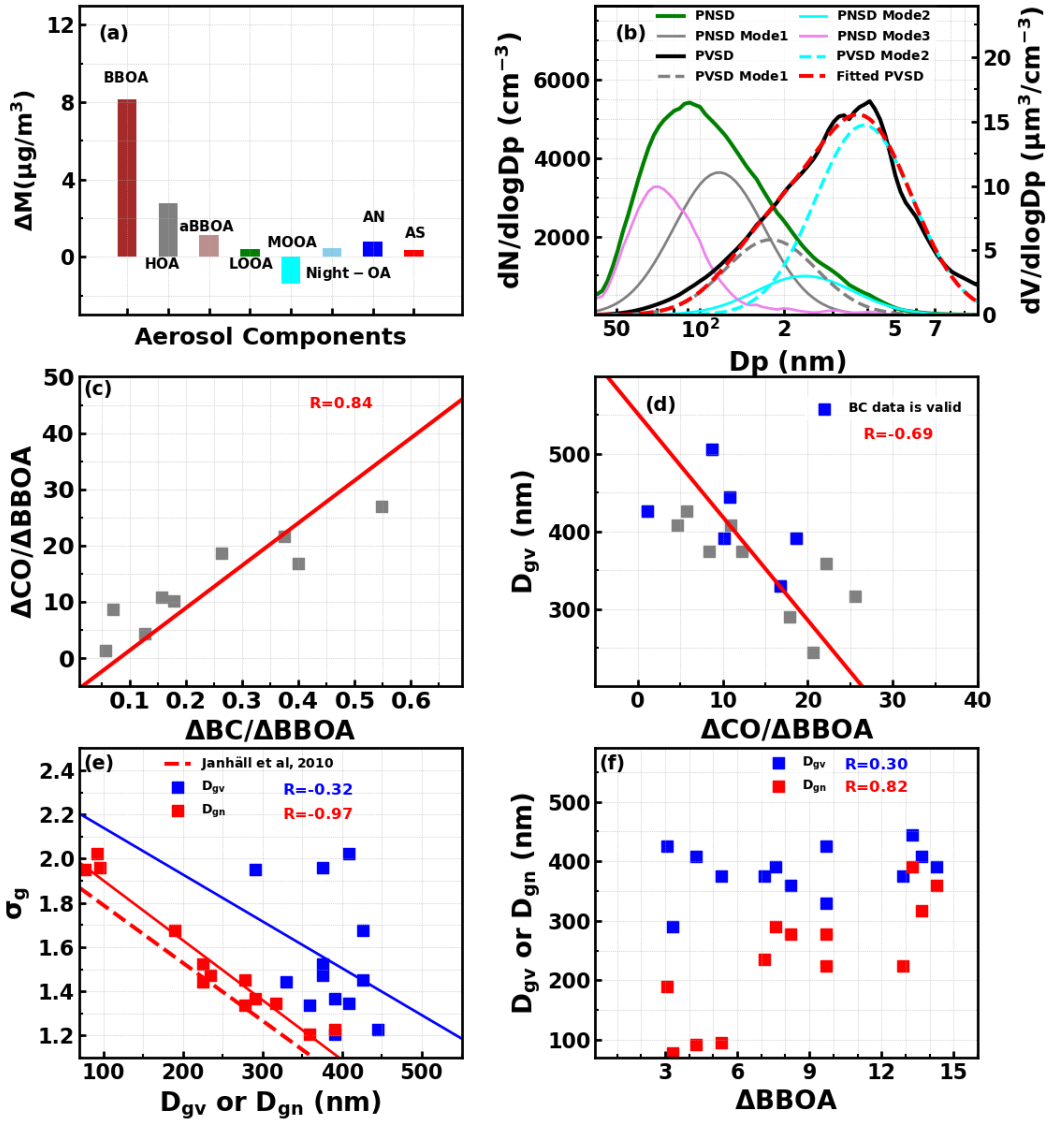

Figure 3. **(a)** Average differences of aerosol components before and end of BBOA spikes; **(b)** Corresponding particle average number and volume size distribution difference (ΔPNSD and ΔPVSD); (c) Relationship between ΔCO/ΔBBOA and ΔBC/ΔBBOA; **(d)** The relationships between identified D_{gv} of BBOA spikes and corresponding ΔCO/ΔBBOA (ppb/(ug/m^3)); **(e)** relationship between retrieved D_{gv} and σ_g, as well as D_{gv} and σ_g. (f) relationships between D_{gv} or D_{gn} and ΔBBOA.

PVSD) calculated as the PNSD and PVSD differnces between those at the BBOA peak concentration and those before the BBOA spikes are shown in Fig.3b, the example of calculating Δ PNSD and Δ PVSD is shown in Fig.S10. The average ΔPVSD can be well fitted using two lognormal modes (Mode 1 and Mode 2), the dominant one is BBOA and another is mostly associated with HOA according to the aerosol mass changes. Geometric mean (D_{gv}) and standard deviation (σ_g) values of the two PVSD lorgnormal modes are 180, 390 and 1.46, 1.5, respectively. In addition, the SP-AMS measurements provides organic aerosol size distributions with vacuum aerodynamic diameter (D_{va}), their average distribution difference of organic aerosols during these spikes are also shown in Fig.S11 and could be

generally well fitted using two lognormal modes of BBOA and HOA. The $D_{gv,Dva}$ and σ_g values of the identified modes were 175, 395 and 1.46, 1.55, respectively. D_{va} and mobility diameter Dp of the SMPS were related through the effective density of particles as $\rho_e = Da/(Dm \times C_S)$, where ρ_e is the aerosol effective density and C_S a factor related to aerosol shape, for which a value of 0.8 was adopted (Jayne et al., 2000). Based on densities of BBOA and HOA introduced in Sect.2.2, identifed D_{gv} of BBOA and HOA from SP-AMS measurements of 395 and 190 nm, which were quite close to the D_{gv} identified from SMPS measurements, further confirming the results from SMPS measurements. The average ΔPNSD is shown in Fig.3b, displaying a number concentrations peak near 90 nm, however, influences of HOA need to be excluded to identify biomass burning PNSD modes. As shown in Fig.3b, converting the identified BBOA and HOA ΔPVSD modes to ΔPNSD modes cannot explain the observed PNSD difference, the remaining mode is lorgnormal and peaks at 70 nm. These results indicate that two modes existed for biomass burning aerosols during this campaign, which is consistent with findings of previous studies (Okoshi et al., 2014;Liu et al., 2020a).

For spikes where ΔBBOA dominated the mass changes, the D_{gv} and σ_g of BBOA PVSD was retrieved by fitting the larger mode of Δ PVSD, with retrieved results shown in Fig.3d and Fig.3e. The retrieved D_{gv} ranged from 245 nm to 505 nm with an average of 380 nm. Physicochemical properties of biomass burning emissions depended largly on combustion conditions. BC/BBOA ratio is a proxy of biomass combustion efficiencies (McClure et al., 2020), and it was found that ΔCO/ΔBBOA was highly correlated with ΔBC/ΔBBOA (Fig.3c, R=0.84). Thus, ΔCO/ΔBBOA was also used as a proxy for combustion efficiency in this study. Higher ΔCO/ΔBBOA corresponds to higher combustion efficiency. Retrieved D_{gv} values were moderatly but negatively correlated with ΔCO/ΔBBOA (R=-0.69), and a linear relationship D_{gv}=551-13.3×ΔCO/ΔBBOA was derived. This result is qualitively consistent with previous studies that biomass burning aerosols were mainly in the accumulation mode and their average sizes generally decreased as the combustion efficiency increases (Reid and Hobbs, 1998;Janhäll et al., 2010). Retreived σ_g ranges from 1.2 to 2.0 with an average of 1.5, and is negatively and weakly correlated with D_{gv} (R=-0.32). Reid et al. (2005b) reported that D_{gv} is typicaly in the range of 250 to 300 nm with the σ_g on the order of 1.6 to 1.9 for freshly generated smoke, and 30-80 nm larger for aged smoke with smaller σ_g (1.4 to 1.6). Levin et al. (2010) performed laboratory combustion of various wildland fuels, and reported D_{gv} of 200 to 570 nm and σ_g of 1.68 to 2.97. The

369 average D_{gv} and σ_g is near the reported D_{gv} range by Reid et al. (2005b) for aged smoke. Geometric
370 mean of PNSD (D_{gn}) values are converted from retrieved D_{gv} and σ_g and also shown in Fig.3e. D_{gn}
371 ranges from 88 to 391 nm with an average of 235 nm. The average D_{gn} is similar with the reported
372 aveage D_{gn} of aged smoke but the range even beyond the range (100-300 nm) for both fresh and aged
373 smokes reported by Janhäll et al. (2010) in which literature published D_{gn} are reviewed, and also
374 beyond the range (about 130-240 nm) reported in Laing et al. (2016) for aged biomass burning aerosol
375 from wildfires in Siberia and the Western USA. Similar with resuls of Janhäll et al. (2010), σ_g is highly
376 but negatively correlated with D_{gn} (R=-0.97). The derived linear relationship σ_g=2.17-0.0027×D_{gn} is
377 close to that reported in Janhäll et al. (2010) (Fig.3e). Janhäll et al. (2010) defined the fresh smoke as
378 plumes younger than 1 h, but aged smoke are mostly plumes older than one day. The aged smoke in
379 Laing et al. (2016) were also transported over 4-10 days. However, the smoke plumes reported in this
380 stduy occurred during supper cooking time, and swept over the observation site last about 1-3h (from
381 the begining to BBOA concentration fall back the background levels) which are consistent the time
382 need for cooking, which means that the age of plumes are on ther oder of hour and near freashly
383 emmited. This is indirectly confimed by the observed changes in particle number concentrations that
384 small aitken mode dominate the particle number contrations (Fig.3b), bacuase coagulation is quick and
385 should cause a significant decrease in number concentrations of Aitken mode aerosols in times scales
386 of hours (Sakamoto et al., 2015;Laing et al., 2016;Sakamoto et al., 2016). These results demonstrate
387 that D_{gn} and D_{gv} varies over a wide range for near freshly emitted BBOA from vegetation fire smokes.
388 Laing et al. (2016) reported that D_{gn} was highly correlated with plume aerosol mass concentrations
389 (PM), but not with any normalized variable such as ΔPM/ΔCO. Simlar results were obtained in this
390 study (Fig.3f). The derived D_{gn} was weakly correlated (R=-0.21) with ΔCO/ΔBBOA, but highly
391 correlated with ΔBBOA (R=0.82). The new finding here is that D_{gv} correlated obviously with
392 ΔCO/ΔBBOA, but weakly with ΔBBOA. As discussed in implications, BBOA volume size
393 distributions determine BBOA bulk optical proeprties thus accurate representations of BBOA volume
394 size dsitrutbuions in climate models might be more important than accurate representations of BBOA
395 number size dsitrutbuions.
396
397 **3.3 BBOA Mass Scattering Efficiency and retrieval of the real part of BBOA refractive index**

The measured aerosol scattering coefficients at 525 nm ($\sigma_{sp,525}$) during BBOA spikes were used to calculate the MSEs using the differential method, thereby retrieving the real part of BBOA refractive index (m_R) on the basis of Mie theory. Truncation error, non-ideality of light source and RH conditions need to be corrected in the calculation of $\sigma_{sp,525}$ values under dry condition. The truncation error and non-ideality of light source was corrected using the empirical formula provided by Qiu et al. (2021). RH_0 in the dry nephelometer was in the range of 20% to 45% with an average of 31%, and corrected by considering measured aerosol optical hygroscopicity through $\sigma_{sp,525}=\sigma_{sp,525,measured}/(1+\kappa_{sca} \times \frac{RH_0}{100-RH_0})$, where κ_{sca} is the optical hygroscopicity parameter derived from aerosol light scattering enhancement factor measurements (Kuang et al., 2017). To quantify MSE_{BBOA}, MSEs of other aerosol components are needed. Using the paired campaign average size distributions of AS and AN (Fig.S3), MSEs of AS and AN was calculated as 4.6 and 4.8 m^2/g, which were identical with those identified by Tao et al. (2019) during autumn at an urban area in this region, but much higher than average values reported in Hand and Malm (2007). Through the analysis of the OA distribution measured by SP-AMS, it was found that the size distribution of SOA can be represented by two lognormal modes (Fig.S4). One is aBBOA, and the other one includes MOOA, Night-OA, and MOOA. Thus, MSE of MOOA, Night-OA, LOOA (MSE_{SOA}) was determined to be 6.3 m^2/g, and MSE_{aBBOA} was 4.5 m^2/g. MSE_{HOA} was calculated to be 3.2 m^2/g using the size distribution identified in Fig.3b. MSE_{BC} was calculated as 2.8 m^2/g using the average normalized C_x fragments distributions, which was also very close to the MSE of elemental carbon determined by Tao et al. (2019) (2.6 m^2/g). The changes of aerosol scattering coefficients associated only with BBOA can be calculated as $\Delta\sigma_{sp,BBOA}=\Delta\sigma_{sp,measured}$ -ΔAS × MSE_{AS}-ΔAN × MSE_{AN}-ΔHOA × MSE_{HOA}-ΔBC × MSE_{BC}-ΔaBBOA × MSE_{aBBOA}–(ΔNight-OA+ΔMOOA+ΔLOOA) × MSE_{SOA}. More details about MSE calculations of these components can be found in Sect.S1. In addition, to minimize the influences of uncertainties of used MSEs of other aerosol components on MSE_{BBOA} derivations, only spikes with sum changes of ΔAS, ΔAN, ΔNight-OA, ΔMOOA, ΔLOOA and ΔaBBOA accounting for less than 25% of Δ BBOA were used. Average changes of aerosol components for these spikes are shown in Fig.4a, with changes of most individual aerosol components being almost negeligible.

As shown in Fig.4b, the derived $\Delta\sigma_{sp,525}$ associated with BBOA was highly correalted with Δ BBOA (R=0.91). MSE_{BBOA} ranged from 3.1 to 7.5 m^2/g with an average of 5.3 m^2/g. Reid et al. (2005a)

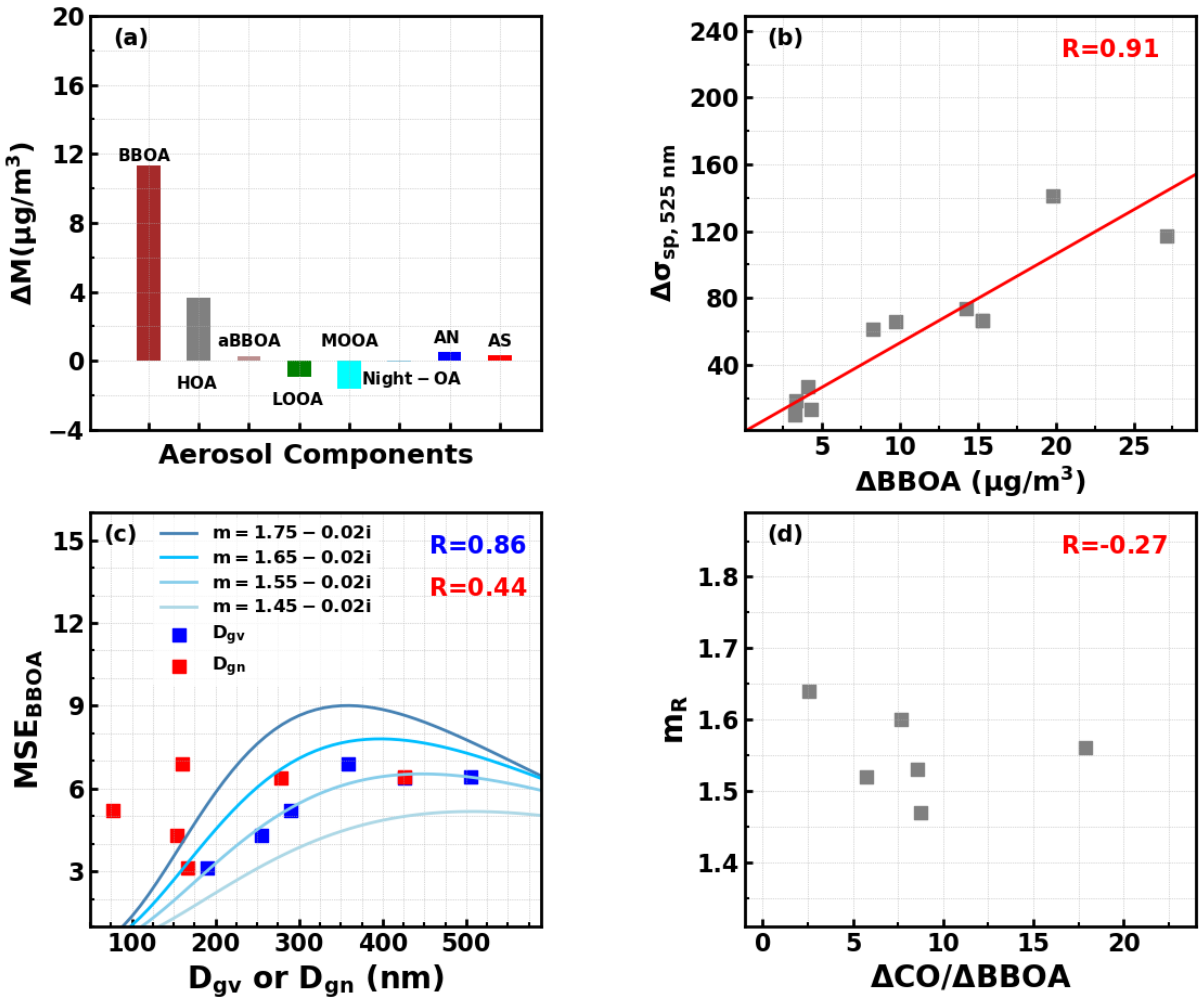

Figure 4. (a) Average differences of aerosol components between nearest background and the peak of BBOA spikes; (b) Relationships between derived $\Delta\sigma_{sp}$ at 525 nm only associated with BBOA and Δ BBOA; (c) Relationships between retrieved MSE_{BBOA} and D_{gn} or D_{gv}; (d) Relationship between retrieved m_R and ΔCO/ΔBBOA.

reviewed the MSEs of biomass burning (MSE_{BB}) aerosols and reported a range of 3.2-4.2 m^2/g for temperate and boreal fresh smoke, and larger for corresponding aged smoke (4.3 m^2/g). McMeeking et al. (2005) theoretically calculated the MSEs of smoke-influenced aerosols and reported a MSE range of 3-6 m^2/g. Levin et al. (2010) conducted MSE_{BB} measurements of fresh biomass burning smokes of various fuel types, reported a MSE_{BB} range of 1.6 to 5.7 m^2/g. Laing et al. (2016) reported a MSE_{BB} range of 2.5 to 4.7 for aged biomass burning aerosols of wildfires, and similar range was reported by Briggs et al. (2017). However, no study has specifically investigated MSE_{BBOA} variations, which are very crucial for biomass burning aerosol climate effects simulations, since aerosol components in models are usually separately represented (Riemer et al., 2019). Although organic aerosols usually dominate mass concentration of biomass burning aerosols, the reported MSE_{BBOA} range is generally

437 higher than previously reported MSE_{BB} ranges, which are likely associated with the fact that MSE_{BB}
438 includes influences of low scattering efficiency components such as BC. Another reason for this is that
439 the identified geometric mean size of BBOA in this study was generally larger than those reported
440 before. Many studies have shown that aerosol size distribution have crucial impacts on MSE variations
441 (Hand and Malm, 2007). Both results of Levin et al. (2010) and Laing et al. (2016) have reported that
442 MSE_{BB} of biomass burning aerosols were highly correlated with D_{gn}. The relationship between
443 MSE_{BBOA} and D_{gn} as well as D_{gv} were investigated (Fig.4c, only six points with both D_{gv} and σ_g
444 retrieval are available). Unlike results of previous studies, MSE_{BBOA} were positively but weakly
445 correlated with D_{gn} (R=0.44). However, MSE_{BBOA} were highly correlated to D_{gv}(R=0.86), and
446 exhibited non-linear response with the increase of D_{gv}. The non-linear increase phenomenon was
447 reported first but confirmed by Mie theory simulations by assuming a fixed σ_g of 1.5 under varying
448 conditions of D_{gv} and refractive index (Fig.4c).

449 Aerosol refractive index was a fundamental parameter in simulating aerosol optical properties in
450 models. However, aerosol refractive index investigations specific to BBOA is scarce because the direct
451 retrieval of aerosol refractive index at least needs accurate and simultaneous representations of
452 MSE_{BBOA}, BBOA density and BBOA size distribution shape. Only few studies have indirectly
453 retrieved m_R of biomass burning related aerosols. For example, McMeeking et al. (2005) and Levin et
454 al. (2010) have retrieved m_R of biomass burning or smoke-influenced aerosols through using an
455 iterative algorithm to match measured size distributions of different principles (mobility-related size
456 versus optical size), reported m_R ranges were 1.56 to 1.59 and 1.41 to 1.61, respectively. In this study,
457 m_R values of BBOA were retrieved using Mie theory with MSE_{BBOA}, D_{gn}, σ_g and BBOA density as
458 inputs as introduced in Sect.1.4 of the supplement. This method assumes the external mixing of BBOA
459 with other aerosol components which due to freshly emitted charaterisitcs and dominant contribution
460 of BBOA to observed mass changes for identified biomass burning plumes. Note that the retrieval of
461 m_R would also be affected by the imaginary part of BBOA refractive index ($m_{i,BBOA}$), and the $m_{i,BBOA}$
462 parameterization as a function of ΔCO/ΔBBOA introduced in the next section was used. Retrieved m_R
463 ranges from 1.47 to 1.64 with an average of 1.56. If m_R changes from 1.47 to 1.64 can result in a double
464 MSE_{BBOA} for given BBOA size distributions. Thus, reported $m_{R,BBOA}$ range was wide with respect to
465 MSE simulations and needs to be carefully parameterized in climate modes. BBOA refrative index is
466 determined by its chemical structure thus its variation might be associated with fire combustion

conditions. The relationship between $m_{R,BBOA}$ and ΔCO/ΔBBOA was further investigated and shown in Fig.4d. For ΔCO/ΔBBOA below 10 ppb/$\mu g \cdot m^3$, m_R was negatively correlated with ΔCO/ΔBBOA (R=-0.71) thus like ΔBC/ΔBBOA, which however, was not as significant (R=-0.27). These results demonstrate that fire combustion conditions might have significant impacts on $m_{R,BBOA}$, however, needs further investigation.

3.4 BBOA mass absorption efficiency and parameterizations of the spectral dependence of imaginary part of BBOA refractive index

Derived BrC absorptions of BBOA spikes were used to calculate MAE_{BBOA} and retrieve $m_{i,BBOA}$ in combination of retrieved BBOA size distributions using Mie theory. Average changes of organic aerosol components for spikes with available σ_{BrC} values are shown in Fig.5a. ΔBBOA dominated the mass changes, however, non-negligible changes for aBBOA, HOA and MOOA. The average MAE_{HOA}, MAE_{aBBOA} and MAE_{MOOA} are estimated using multilinear regression for all data points as shown in Fig.S12 with values at 370 nm of 0.1, 0.96 and 0.9 m^2/g, respectively. Thus the $\Delta\sigma_{BrC,BBOA}$ can be derived as $\Delta\sigma_{BrC,BBOA}(\lambda)=\Delta\sigma_{BrC,derived}$ - ΔHOA×$MAE_{HOA}(\lambda)$ - ΔaBBOA×$MAE_{aBBOA}(\lambda)$ – ΔMOOA×$MSE_{MOOA}(\lambda)$. As shown in Fig.5b, $\Delta\sigma_{BrC,BBOA}$ was moderately correalted with ΔBBOA (R=0.65), suggesting $MAE_{BBOA}=\Delta\sigma_{BrC,BBOA}$/ΔBBOA differs much among identified plumes. Derived MAE_{BBOA} exhibited strong wavelength dependence and average values at wavelengths of 370, 470, 520, 590, and 660 nm were 2.46,0.99,0.53,0.28, 0.11 m^2/g, respectively. Fig.5c shows the spectral dependence of MAE_{BBOA} and retrieved $m_{i,BBOA}(\lambda)$, and formula form that parameterize the spectral dependence was consistent with previous studies (Saleh et al., 2014). BBOA absorption properties depended largely on combustion conditions, consistent with results of previous studies (Saleh et al., 2014;Lu et al., 2015;Pokhrel et al., 2016;Xie et al., 2017;Cheng et al., 2019;McClure et al., 2020), both MAE_{BBOA} and retrieved $m_{i,BBOA}(520)$ was highly and linearly correlated with ΔBC/ΔBBOA (Fig.5d and Fig.5e). Results regarding $m_{i,BBOA}(\lambda)$ parameterizations as a function of ΔBC/ΔBBOA of previous studies are also shown in Fig.5e. Results of Saleh et al. (2014) and Lu et al. (2015) at 550 nm were higher for ΔBC/ΔBBOA in the range of 0.05 to 0.4. Curve of McClure et al. (2020) well described the $m_{i,BBOA}$ variations for ΔBC/ΔBBOA less than 0.2. The $m_{i,BBOA}$ spectral dependence parameter w_{BBOA}

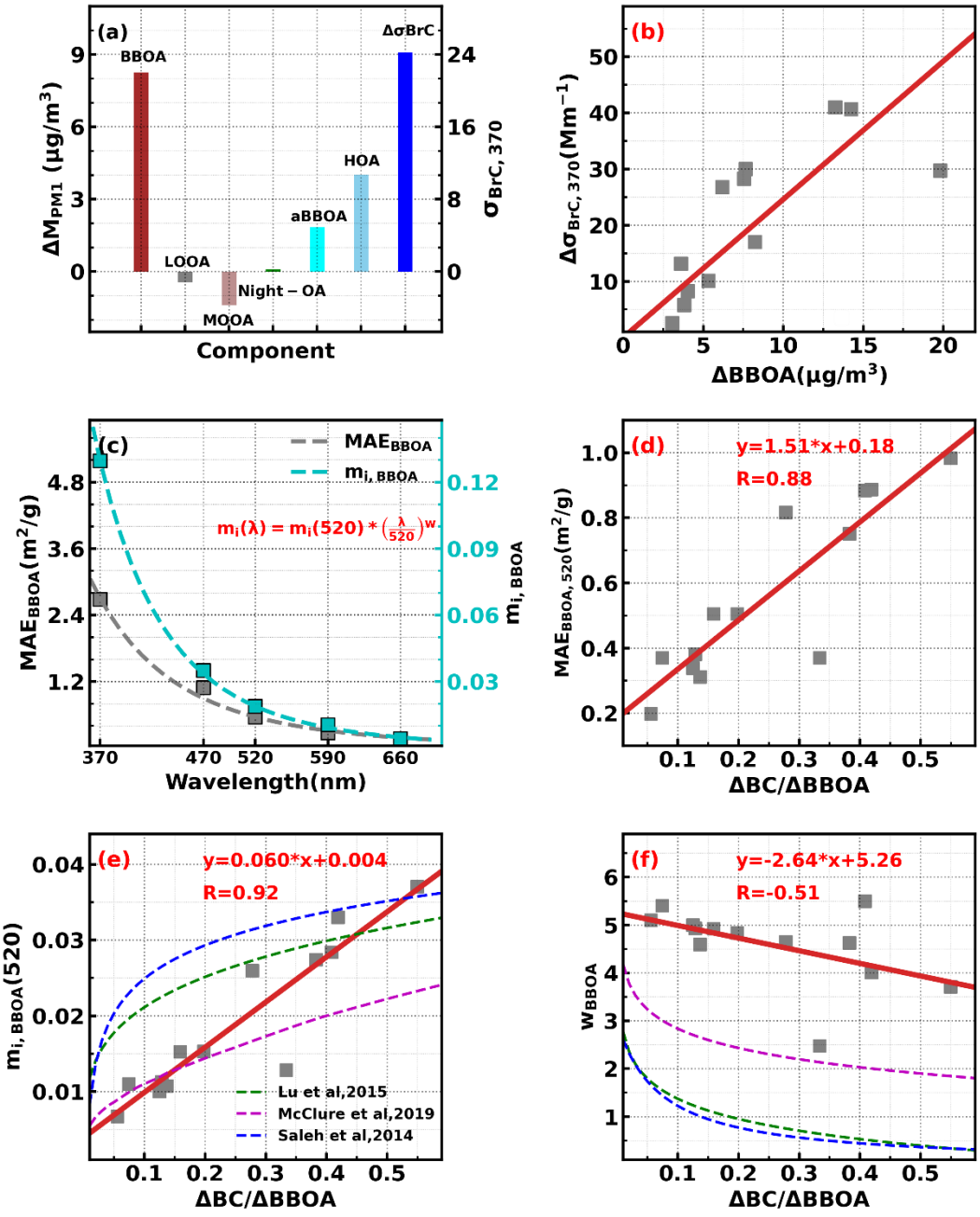

Figure 5. **(a)** Average changes of organic aerosol components for BBOA spikes when BC measurements are available; **(b)**Relationships between derived $\Delta\sigma_{Brc}$ at 525 nm only associated with BBOA and Δ BBOA; **(c)**Average spectral dependence of MAE_{BBOA} and $m_{i,BBOA}$; **(d)** Relationship between MAE_{BBOA} at 525 nm and ΔBC/ΔBBOA; **(e)** Relationship between $m_{i,BBOA}$ at 520 nm and ΔBC/ΔBBOA; **(f)** Relationship between the spectral dependence parameter w_{BBOA} and ΔBC/ΔBBOA.

ranged from 2.5 to 5.5 with an average of 4.7, was linearly and negatively correlated to ΔBC/ΔBBOA and much higher than those reported in Saleh et al. (2014) and Lu et al. (2015). Note that the paraeterization schemes established in Saleh et al. (2014) and Lu et al. (2015) were based on datasets with most data points with BC/BBOA<0.1. The w_{BBOA} was also higher than the fitted line of McClure

et al. (2020), however, was actutally consistent with the w_{BBOA} range reported in Fig.5c of McClure et al. (2020) for a BC/OA range of 0.1 to 0.55. This result implies that a single formula that parameterize $m_{i,BBOA}$ over a wide BC/BBOA (combustion efficiency) range might lead to significant bias for specific BC/BBOA ranges. As shown in Fig.1 of Lu et al. (2015), field-based $m_{i,BBOA}$ retrievals for BC/BBOA>0.1 are quite scarce which hinder the accurate parameterization of $m_{i,BBOA}$ within the BC/BBOA range of this study. The combination of $m_{i,BBOA}(520)$ and w_{BBOA} shown in Fig.5e and Fig.5f would bring a new parameterization scheme of $m_{i,BBOA}(\lambda)$ spetral dependece, which filled the gap for field-based BBOA absorptivity paramterizations of BC/BBOA>0.1.

4. Implications for simulating climate effects of BBOA

Findings of BBOA size distributions, real and imginary parts of BBOA refractive index in this study have important implications for climate modelling of BBOA radiative effects. The volume dominant mode of biomass burning aerosols contribute dominantly to aerosol mass, which are most important for BBOA scattering and absoprtion properties. The volume dominant mode also contributed dominantly to number concentration for diameter range of >150 nm, and this diameter range played the dominant role in BBOA aerosols as cloud condensation nucei (Chen et al., 2019). However, previous studies usually parameterized number geometric mean diameter D_{gn} as a function of combustion conditions. It was found that BBOA mass scattering efficiency correlated well with the volume geometric mean diameter D_{gv}, but correlated poorly with D_{gn}, which was in contradiction with previous results (Levin et al., 2010;Laing et al., 2016) that BBOA mass scattering efficiency was highly correlated with D_{gn}. However, the simulation results shown in Fig.S13 explained the contrast, that aerosol scattering efficiency were very sensitive to σ_g changes for fixed D_{gn}, however, are much less sensitive to σ_g changes for D_{gv}, and retreived σ_g varied over a wide range from 1.2 to 2 in this study. In addition, it was found that D_{gn} correlated poorly with normalized parameters such as ΔCO/ΔBBOA, whereas D_{gv} correlated highly with ΔCO/ΔBBOA . Therefore, representating BBOA volume size distribution of the volume dominant mode as a function of combustion conditions in climate models might be a better choice if using only one size distribution mode (Stier et al., 2005;Dentener et al., 2006), however needs further and synthesized research on this topic. In view of this, on the basis of the relationships between ΔCO/ΔBBOA and ΔBC/ΔBBOA, the D_{gv} were parameterized as D_{gv}=632-1000×ΔBC/ΔBBOA, and might be applicable in climate models (Saleh, 2020).

The real part of BBOA refractive $m_{R,BBOA}$ was fundamental parameter for simulating BBOA

scattering properties in Climate models, however, a constant was usually used due to the lack of adequate parameterizations (Brown et al., 2021). Significant changes were found in $m_{R,BBOA}$ in this study (1.47 to 1.64), and the variations were likely closely associated with changes in fire combustion conditions represented by ΔCO/ΔBBOA. For BBOA refractive index, the imaginary part ($m_{i,BBOA}$) are currently recommended to be parameterized as a function of BC/BBOA ratio (Saleh et al., 2014), which is supported by results of several studies (Lu et al., 2015;McClure et al., 2020). Results of this study suggests that it might be also feasible to parameterize $m_{i,BBOA}$ as a function of BC/BBOA, however, needs further comprehensive investigations.

The immaginary part of BBOA refractive index, $m_{i,BBOA}$, plays crucial role in representing BBOA absorptivity in climate models. Linear relationships between $m_{i,BBOA}$ as well as the spectral dependence parameter w_{BBOA} and BC/OA are reported for the first time in this study. The observed BC/OA ratio (0.05 to 0.55) locates within the upper range of previously reported BC/OA values. Few measurements regarding aerosol refractive index and size-distributions are available in this BC/OA range, and no researches have focused on parameterizations of BBOA refractive index in this specific BC/OA range, thus results of this study have partially filled this gap. Results of McClure et al. (2020) demonstate that a sigmoidal curve fitts well the $m_{i,BBOA}$ variations for a wide range of BC/OA ratio (10^{-5} to 10), however the $m_{i,BBOA}$ variations are not well captured by the fitted curve for BC/OA>0.1. We recommend for more sophisticated parameterizations of $m_{i,BBOA}$ under different BC/OA ranges.

Data availability. The data used in this study are available from the corresponding author upon request

Ye Kuang (kuangye@jnu.edu.cn) and Shan Huang (shanhuang_eci@jnu.edu.cn)

Competing interests. The authors declare that they have no conflict of interest.

Author Contributions.

YK and SH designed this experiment, YK conceived and led this research. BL and YK wrote the manuscript. SH lead the SP-AMS measurements and particle number size distribution measurements. SH performed the PMF analysis and C_x fragment analysis, revised the manuscript. MS and BY planned this campaign. DC and DY provided authority of conducting the campaign in Heshan supersite and gave data availability from the site. All other coauthors have contributed to this paper in different ways.

Acknowledgments

This work is supported by the National Natural Science Foundation of China (grant No. 41805109, 41807302), National Key Research and Development Program of China (grant No. 2017YFC0212803, 2016YFC0202206), Key-Area Research and Development Program of Guangdong Province (grant No. 2019B110206001), Special Fund Project for Science and Technology Innovation Strategy of Guangdong Province (grant No.2019B121205004), Guangdong Natural Science Funds for Distinguished Young Scholar (grant No. 2018B030306037) and Guangdong Innovative and Entrepreneurial Research Team Program (grant No. 2016ZT06N263).

References

Bond, T. C., Doherty, S. J., Fahey, D. W., Forster, P. M., Berntsen, T., DeAngelo, B. J., Flanner, M. G., Ghan, S., Kärcher, B., Koch, D., Kinne, S., Kondo, Y., Quinn, P. K., Sarofim, M. C., Schultz, M. G., Schulz, M., Venkataraman, C., Zhang, H., Zhang, S., Bellouin, N., Guttikunda, S. K., Hopke, P. K., Jacobson, M. Z., Kaiser, J. W., Klimont, Z., Lohmann, U., Schwarz, J. P., Shindell, D., Storelvmo, T., Warren, S. G., and Zender, C. S.: Bounding the role of black carbon in the climate system: A scientific assessment, Journal of Geophysical Research: Atmospheres, 118, 5380-5552, https://doi.org/10.1002/jgrd.50171, 2013.

Briggs, N. L., Jaffe, D. A., Gao, H., Hee, J. R., Baylon, P. M., Zhang, Q., Zhou, S., Collier, S. C., Sampson, P. D., and Cary, R. A.: Particulate Matter, Ozone, and Nitrogen Species in Aged Wildfire Plumes Observed at the Mount Bachelor Observatory, Aerosol and Air Quality Research, 16, 3075-3087, 10.4209/aaqr.2016.03.0120, 2017.

Brown, H., Liu, X., Pokhrel, R., Murphy, S., Lu, Z., Saleh, R., Mielonen, T., Kokkola, H., Bergman, T., Myhre, G., Skeie, R. B., Watson-Paris, D., Stier, P., Johnson, B., Bellouin, N., Schulz, M., Vakkari, V., Beukes, J. P., van Zyl, P. G., Liu, S., and Chand, D.: Biomass burning aerosols in most climate models are too absorbing, Nature communications, 12, 277, 10.1038/s41467-020-20482-9, 2021.

Chen, L., Li, Q., Wu, D., Sun, H., Wei, Y., Ding, X., Chen, H., Cheng, T., and Chen, J.: Size distribution and chemical composition of primary particles emitted during open biomass burning processes: Impacts on cloud condensation nuclei activation, Science of The Total Environment, 674, 179-188, https://doi.org/10.1016/j.scitotenv.2019.03.419, 2019.

Cheng, Z., Atwi, K., Onyima, T., and Saleh, R.: Investigating the dependence of light-absorption properties of combustion carbonaceous aerosols on combustion conditions, Aerosol Science and Technology, 53, 419-434, 10.1080/02786826.2019.1566593, 2019.

Collaud Coen, M., Weingartner, E., Apituley, A., Ceburnis, D., Fierz-Schmidhauser, R., Flentje, H., Henzing, J. S., Jennings, S. G., Moerman, M., Petzold, A., Schmid, O., and Baltensperger, U.: Minimizing light absorption measurement artifacts of the Aethalometer: evaluation of five correction algorithms, Atmos. Meas. Tech., 3, 457-474, 10.5194/amt-3-457-2010, 2010.

de Sa, S. S., Rizzo, L. V., Palm, B. B., Campuzano-Jost, P., Day, D. A., Yee, L. D., Wernis, R., Isaacman-VanWertz, G., Brito, J., Carbone, S., Liu, Y. J. J., Sedlacek, A., Springston, S., Goldstein, A. H., Barbosa, H. M. J., Alexander, M. L., Artaxo, P., Jimenez, J. L., and Martin, S. T.: Contributions of biomass-burning, urban, and biogenic emissions to the concentrations and light-absorbing properties of particulate matter in central Amazonia during the dry season, Atmospheric Chemistry and Physics, 19, 7973-8001, 10.5194/acp-19-7973-2019, 2019.

Dentener, F., Kinne, S., Bond, T., Boucher, O., Cofala, J., Generoso, S., Ginoux, P., Gong, S., Hoelzemann, J. J., Ito, A., Marelli, L., Penner, J. E., Putaud, J. P., Textor, C., Schulz, M., van der Werf, G. R., and Wilson, J.: Emissions of primary aerosol and precursor gases in the years 2000 and 1750 prescribed data-sets for AeroCom, Atmos. Chem. Phys., 6, 4321-4344, 10.5194/acp-6-4321-2006, 2006.

Drinovec, L., Močnik, G., Zotter, P., Prévôt, A. S. H., Ruckstuhl, C., Coz, E., Rupakheti, M., Sciare, J., Müller, T., Wiedensohler, A., and Hansen, A. D. A.: The "dual-spot" Aethalometer: an improved measurement of aerosol black carbon with real-time loading compensation, Atmospheric Measurement Techniques, 8, 1965-1979, 10.5194/amt-8-1965-2015, 2015a.

Drinovec, L., Mocnik, G., Zotter, P., Prevot, A. S. H., Ruckstuhl, C., Coz, E., Rupakheti, M., Sciare, J., Muller, T., Wiedensohler, A., and Hansen, A. D. A.: The "dual-spot" Aethalometer: an improved measurement of aerosol black carbon with real-time loading compensation, Atmospheric Measurement Techniques, 8, 1965-1979, 10.5194/amt-8-1965-2015, 2015b.

Gysel, M., Crosier, J., Topping, D. O., Whitehead, J. D., Bower, K. N., Cubison, M. J., Williams, P. I., Flynn, M. J., McFiggans, G. B., and Coe, H.: Closure study between chemical composition and hygroscopic growth of aerosol particles during TORCH2, Atmos. Chem. Phys., 7, 6131-6144, 10.5194/acp-7-6131-2007, 2007.

Hand, J. L., and Malm, W. C.: Review of aerosol mass scattering efficiencies from ground-based measurements since 1990, Journal of Geophysical Research: Atmospheres, 112, https://doi.org/10.1029/2007JD008484, 2007.

Hecobian, A., Liu, Z., Hennigan, C. J., Huey, L. G., Jimenez, J. L., Cubison, M. J., Vay, S., Diskin, G. S., Sachse, G. W., Wisthaler, A., Mikoviny, T., Weinheimer, A. J., Liao, J., Knapp, D. J., Wennberg, P. O., Kürten, A., Crounse, J. D., Clair, J. S., Wang, Y., and Weber, R. J.: Comparison of chemical characteristics of 495 biomass burning plumes intercepted by the NASA DC-8 aircraft during the ARCTAS/CARB-2008 field campaign, Atmos. Chem. Phys., 11, 13325-13337, 10.5194/acp-11-13325-2011, 2011.

Hoffer, A., Tóth, Á., Pósfai, M., Chung, C. E., and Gelencsér, A.: Brown carbon absorption in the red and near-infrared spectral region, Atmos. Meas. Tech., 10, 2353-2359, 10.5194/amt-10-2353-2017, 2017.

Janhäll, S., Andreae, M. O., and Pöschl, U.: Biomass burning aerosol emissions from vegetation fires: particle number and mass emission factors and size distributions, Atmos. Chem. Phys., 10, 1427-1439, 10.5194/acp-10-1427-2010, 2010.

Jayne, J. T., Leard, D. C., Zhang, X., Davidovits, P., Smith, K. A., Kolb, C. E., and Worsnop, D. R.: Development of an Aerosol Mass Spectrometer for Size and Composition Analysis of Submicron Particles, Aerosol Science and Technology, 33, 49-70, 10.1080/027868200410840, 2000.

Kasthuriarachchi, N. Y., Rivellini, L.-H., Adam, M. G., and Lee, A. K. Y.: Light Absorbing Properties of Primary and Secondary Brown Carbon in a Tropical Urban Environment, Environ. Sci. Technol., 54, 10808-10819, 10.1021/acs.est.0c02414, 2020.

Kuang, Y., Zhao, C., Tao, J., Bian, Y., Ma, N., and Zhao, G.: A novel method for deriving the aerosol hygroscopicity parameter based only on measurements from a humidified nephelometer system, Atmos. Chem. Phys., 17, 6651-6662, 10.5194/acp-17-6651-2017, 2017.

Kuang, Y., He, Y., Xu, W., Zhao, P., Cheng, Y., Zhao, G., Tao, J., Ma, N., Su, H., Zhang, Y., Sun, J., Cheng, P., Yang, W., Zhang, S., Wu, C., Sun, Y., and Zhao, C.: Distinct diurnal variation in organic aerosol hygroscopicity and its relationship with oxygenated organic aerosol, Atmos. Chem. Phys., 20, 865-880, 10.5194/acp-20-865-2020, 2020.

Kuang, Y., Huang, S., Xue, B., Luo, B., Song, Q., Chen, W., Hu, W., Li, W., Zhao, P., Cai, M., Peng, Y., Qi, J., Li, T., Wang, S., Chen, D., Yue, D., Yuan, B., and Shao, M.: Contrasting effects of secondary organic aerosol formations on organic aerosol hygroscopicity, Atmos. Chem. Phys., 21, 10375-10391, 10.5194/acp-21-10375-2021, 2021.

Kuwata, M., Zorn, S. R., and Martin, S. T.: Using Elemental Ratios to Predict the Density of Organic Material Composed of Carbon, Hydrogen, and Oxygen, Environmental science & technology, 46, 787-794, 10.1021/es202525q, 2012.

Lack, D. A., and Cappa, C. D.: Impact of brown and clear carbon on light absorption enhancement, single scatter albedo and absorption wavelength dependence of black carbon, Atmospheric Chemistry and Physics, 10, 4207-4220, 10.5194/acp-10-4207-2010, 2010.

Laing, J. R., Jaffe, D. A., and Hee, J. R.: Physical and optical properties of aged biomass burning aerosol from wildfires in Siberia and the Western USA at the Mt. Bachelor Observatory, Atmos. Chem. Phys., 16, 15185-15197, 10.5194/acp-16-15185-2016, 2016.

Laskin, A., Laskin, J., and Nizkorodov, S. A.: Chemistry of Atmospheric Brown Carbon, Chemical Reviews, 115, 4335-4382, 10.1021/cr5006167, 2015.

Levin, E. J. T., McMeeking, G. R., Carrico, C. M., Mack, L. E., Kreidenweis, S. M., Wold, C. E., Moosmüller, H., Arnott, W. P., Hao, W. M., Collett Jr, J. L., and Malm, W. C.: Biomass burning smoke aerosol properties measured during Fire Laboratory at Missoula Experiments (FLAME), Journal of Geophysical Research: Atmospheres, 115, https://doi.org/10.1029/2009JD013601, 2010.

Li, Z. J., Tan, H. B., Zheng, J., Liu, L., Qin, Y. M., Wang, N., Li, F., Li, Y. J., Cai, M. F., Ma, Y., and Chan, C. K.: Light absorption properties and potential sources of particulate brown carbon in the Pearl River Delta region of China, Atmospheric Chemistry and Physics, 19, 11669-11685, 10.5194/acp-19-11669-2019, 2019.

Liu, D. T., Li, S. Y., Hu, D. W., Kong, S. F., Cheng, Y., Wu, Y. Z., Ding, S., Hu, K., Zheng, S. R., Yan, Q., Zheng, H., Zhao, D. L., Tian, P., Ye, J. H., Huang, M. Y., and Ding, D. P.: Evolution of Aerosol Optical Properties from Wood Smoke in Real Atmosphere Influenced by Burning Phase and Solar Radiation, Environ. Sci. Technol., 55, 5677-5688, 10.1021/acs.est.0c07569, 2021.

Liu, J., Li, J., Zhang, Y., Liu, D., Ding, P., Shen, C., Shen, K., He, Q., Ding, X., Wang, X., Chen, D., Szidat, S., and Zhang, G.: Source apportionment using radiocarbon and organic tracers for PM2.5 carbonaceous aerosols in Guangzhou, South China: contrasting local- and regional-scale haze events, Environmental science & technology, 48, 12002-12011, 10.1021/es503102w, 2014.

Liu, J., Andersson, A., Zhong, G., Geng, X., Ding, P., Zhu, S., Cheng, Z., Zakaria, M. P., Bong, C. W., Li, J., Zheng, J., Zhang, G., and Gustafsson, Ö.: Isotope constraints of the strong influence of biomass burning to climate-forcing Black Carbon aerosols over Southeast Asia, Science of The Total Environment, 744, 140359, https://doi.org/10.1016/j.scitotenv.2020.140359, 2020a.

Liu, L., Cheng, Y., Wang, S., Wei, C., Pöhlker, M. L., Pöhlker, C., Artaxo, P., Shrivastava, M., Andreae, M. O., Pöschl, U., and Su, H.: Impact of biomass burning aerosols on radiation, clouds, and precipitation over the Amazon: relative importance of aerosol–cloud and aerosol–radiation interactions, Atmos. Chem. Phys., 20, 13283-13301, 10.5194/acp-20-13283-2020, 2020b.

Lu, Z., Streets, D. G., Winijkul, E., Yan, F., Chen, Y., Bond, T. C., Feng, Y., Dubey, M. K., Liu, S., Pinto, J. P., and Carmichael, G. R.: Light Absorption Properties and Radiative Effects of Primary Organic Aerosol Emissions, Environmental science & technology, 49, 4868-4877, 10.1021/acs.est.5b00211, 2015.

McClure, C. D., Lim, C. Y., Hagan, D. H., Kroll, J. H., and Cappa, C. D.: Biomass-burning-derived particles from a wide variety of fuels – Part 1: Properties of primary particles, Atmos. Chem. Phys., 20, 1531-1547, 10.5194/acp-20-1531-2020, 2020.

McMeeking, G. R., Kreidenweis, S. M., Carrico, C. M., Lee, T., Collett Jr., J. L., and Malm, W. C.: Observations of smoke-influenced aerosol during the Yosemite Aerosol Characterization Study: Size distributions and chemical composition, Journal of Geophysical Research: Atmospheres, 110, https://doi.org/10.1029/2004JD005389, 2005.

Okoshi, R., Rasheed, A., Chen Reddy, G., McCrowey, C. J., and Curtis, D. B.: Size and mass distributions of ground-level sub-micrometer biomass burning aerosol from small wildfires, Atmospheric Environment, 89, 392-402, https://doi.org/10.1016/j.atmosenv.2014.01.024, 2014.

Pokhrel, R. P., Wagner, N. L., Langridge, J. M., Lack, D. A., Jayarathne, T., Stone, E. A., Stockwell, C. E., Yokelson, R. J., and Murphy, S. M.: Parameterization of single-scattering albedo (SSA) and absorption Ångström exponent (AAE) with EC / OC

for aerosol emissions from biomass burning, Atmos. Chem. Phys., 16, 9549-9561, 10.5194/acp-16-9549-2016, 2016.
Pratt, K. A., Murphy, S. M., Subramanian, R., DeMott, P. J., Kok, G. L., Campos, T., Rogers, D. C., Prenni, A. J., Heymsfield, A. J., Seinfeld, J. H., and Prather, K. A.: Flight-based chemical characterization of biomass burning aerosols within two prescribed burn smoke plumes, Atmos. Chem. Phys., 11, 12549-12565, 10.5194/acp-11-12549-2011, 2011.
Qin, Y. M., Tan, H. B., Li, Y. J., Li, Z. J., Schurman, M. I., Liu, L., Wu, C., and Chan, C. K.: Chemical characteristics of brown carbon in atmospheric particles at a suburban site near Guangzhou, China, Atmospheric Chemistry and Physics, 18, 16409-16418, 10.5194/acp-18-16409-2018, 2018.
Qiu, J., Tan, W., Zhao, G., Yu, Y., and Zhao, C.: New correction method for the scattering coefficient measurements of a three-wavelength nephelometer, Atmos. Meas. Tech., 14, 4879-4891, 10.5194/amt-14-4879-2021, 2021.
Reid, J. S., and Hobbs, P. V.: Physical and optical properties of young smoke from individual biomass fires in Brazil, Journal of Geophysical Research: Atmospheres, 103, 32013-32030, https://doi.org/10.1029/98JD00159, 1998.
Reid, J. S., Eck, T. F., Christopher, S. A., Koppmann, R., Dubovik, O., Eleuterio, D. P., Holben, B. N., Reid, E. A., and Zhang, J.: A review of biomass burning emissions part III: intensive optical properties of biomass burning particles, Atmos. Chem. Phys., 5, 827-849, 10.5194/acp-5-827-2005, 2005a.
Reid, J. S., Koppmann, R., Eck, T. F., and Eleuterio, D. P.: A review of biomass burning emissions part II: intensive physical properties of biomass burning particles, Atmos. Chem. Phys., 5, 799-825, 10.5194/acp-5-799-2005, 2005b.
Riemer, N., Ault, A. P., West, M., Craig, R. L., and Curtis, J. H.: Aerosol Mixing State: Measurements, Modeling, and Impacts, Reviews of Geophysics, 57, 187-249, https://doi.org/10.1029/2018RG000615, 2019.
Sakamoto, K. M., Allan, J. D., Coe, H., Taylor, J. W., Duck, T. J., and Pierce, J. R.: Aged boreal biomass-burning aerosol size distributions from BORTAS 2011, Atmos. Chem. Phys., 15, 1633-1646, 10.5194/acp-15-1633-2015, 2015.
Sakamoto, K. M., Laing, J. R., Stevens, R. G., Jaffe, D. A., and Pierce, J. R.: The evolution of biomass-burning aerosol size distributions due to coagulation: dependence on fire and meteorological details and parameterization, Atmos. Chem. Phys., 16, 7709-7724, 10.5194/acp-16-7709-2016, 2016.
Saleh, R., Hennigan, C. J., McMeeking, G. R., Chuang, W. K., Robinson, E. S., Coe, H., Donahue, N. M., and Robinson, A. L.: Absorptivity of brown carbon in fresh and photo-chemically aged biomass-burning emissions, Atmos. Chem. Phys., 13, 7683-7693, 10.5194/acp-13-7683-2013, 2013.
Saleh, R., Robinson, E. S., Tkacik, D. S., Ahern, A. T., Liu, S., Aiken, A. C., Sullivan, R. C., Presto, A. A., Dubey, M. K., Yokelson, R. J., Donahue, N. M., and Robinson, A. L.: Brownness of organics in aerosols from biomass burning linked to their black carbon content, Nature Geoscience, 7, 647, 10.1038/ngeo2220
https://www.nature.com/articles/ngeo2220#supplementary-information, 2014.
Saleh, R., Marks, M., Heo, J., Adams, P. J., Donahue, N. M., and Robinson, A. L.: Contribution of brown carbon and lensing to the direct radiative effect of carbonaceous aerosols from biomass and biofuel burning emissions, Journal of Geophysical Research: Atmospheres, 120, 10,285-210,296, https://doi.org/10.1002/2015JD023697, 2015.
Saleh, R.: From Measurements to Models: Toward Accurate Representation of Brown Carbon in Climate Calculations, Current Pollution Reports, 6, 90-104, 10.1007/s40726-020-00139-3, 2020.
Stier, P., Feichter, J., Kinne, S., Kloster, S., Vignati, E., Wilson, J., Ganzeveld, L., Tegen, I., Werner, M., Balkanski, Y., Schulz, M., Boucher, O., Minikin, A., and Petzold, A.: The aerosol-climate model ECHAM5-HAM, Atmos. Chem. Phys., 5, 1125-1156, 10.5194/acp-5-1125-2005, 2005.
Tan, H., Liu, L., Fan, S., Li, F., Yin, Y., Cai, M., and Chan, P. W.: Aerosol optical properties and mixing state of black carbon in the Pearl River Delta, China, Atmospheric Environment, 131, 196-208, https://doi.org/10.1016/j.atmosenv.2016.02.003, 2016.
Tao, J., Zhang, Z., Wu, Y., Zhang, L., Wu, Z., Cheng, P., Li, M., Chen, L., Zhang, R., and Cao, J.: Impact of particle number and mass size distributions of major chemical components on particle mass scattering efficiency in urban Guangzhou in southern China, Atmos. Chem. Phys., 19, 8471-8490, 10.5194/acp-19-8471-2019, 2019.

Tao, J., Surapipith, V., Han, Z., Prapamontol, T., Kawichai, S., Zhang, L., Zhang, Z., Wu, Y., Li, J., Li, J., Yang, Y., and Zhang, R.: High mass absorption efficiency of carbonaceous aerosols during the biomass burning season in Chiang Mai of northern Thailand, Atmospheric Environment, 240, 10.1016/j.atmosenv.2020.117821, 2020.

Wang, J. P., Nie, W., Cheng, Y. F., Shen, Y. C., Chi, X. G., Wang, J. D., Huang, X., Xie, Y. N., Sun, P., Xu, Z., Qi, X. M., Su, H., and Ding, A. J.: Light absorption of brown carbon in eastern China based on 3-year multi-wavelength aerosol optical property observations and an improved absorption Angstrom exponent segregation method, Atmospheric Chemistry and Physics, 18, 9061-9074, 10.5194/acp-18-9061-2018, 2018.

Wang, Q., Saturno, J., Chi, X., Walter, D., Lavric, J. V., Moran-Zuloaga, D., Ditas, F., Pöhlker, C., Brito, J., Carbone, S., Artaxo, P., and Andreae, M. O.: Modeling investigation of light-absorbing aerosols in the Amazon Basin during the wet season, Atmos. Chem. Phys., 16, 14775-14794, 10.5194/acp-16-14775-2016, 2016a.

Wang, X., Heald, C. L., Sedlacek, A. J., de Sa, S. S., Martin, S. T., Alexander, M. L., Watson, T. B., Aiken, A. C., Springston, S. R., and Artaxo, P.: Deriving brown carbon from multiwavelength absorption measurements: method and application to AERONET and Aethalometer observations, Atmospheric Chemistry and Physics, 16, 12733-12752, 10.5194/acp-16-12733-2016, 2016b.

Wu, D., Mao, J., Deng, X., Tie, X., Zhang, Y., Zeng, L., Li, F., Tan, H., Bi, X., Huang, X., Chen, J., and Deng, T.: Black carbon aerosols and their radiative properties in the Pearl River Delta region, Science in China Series D: Earth Sciences, 52, 1152-1163, 10.1007/s11430-009-0115-y, 2009.

Xie, M., Hays, M. D., and Holder, A. L.: Light-absorbing organic carbon from prescribed and laboratory biomass burning and gasoline vehicle emissions, Scientific reports, 7, 7318, 10.1038/s41598-017-06981-8, 2017.

Yang, M., Howell, S. G., Zhuang, J., and Huebert, B. J.: Attribution of aerosol light absorption to black carbon, brown carbon, and dust in China - interpretations of atmospheric measurements during EAST-AIRE, Atmospheric Chemistry and Physics, 9, 2035-2050, DOI 10.5194/acp-9-2035-2009, 2009.

Yu, Z., Cheng, Z., Magoon, G. R., Hajj, O. E., and Saleh, R.: Characterization of light-absorbing aerosols from a laboratory combustion source with two different photoacoustic techniques, Aerosol Science and Technology, 55, 387-397, 10.1080/02786826.2020.1849537, 2021.

Yus-Díez, J., Bernardoni, V., Močnik, G., Alastuey, A., Ciniglia, D., Ivančič, M., Querol, X., Perez, N., Reche, C., Rigler, M., Vecchi, R., Valentini, S., and Pandolfi, M.: Determination of the multiple-scattering correction factor and its cross-sensitivity to scattering and wavelength dependence for different AE33 Aethalometer filter tapes: a multi-instrumental approach, Atmos. Meas. Tech., 14, 6335-6355, 10.5194/amt-14-6335-2021, 2021.

Zhang, A., Wang, Y., Zhang, Y., Weber, R. J., Song, Y., Ke, Z., and Zou, Y.: Modeling the global radiative effect of brown carbon: a potentially larger heating source in the tropical free troposphere than black carbon, Atmos. Chem. Phys., 20, 1901-1920, 10.5194/acp-20-1901-2020, 2020.

Zhang, G., Peng, L., Lian, X., Lin, Q., Bi, X., Chen, D., Li, M., Li, L., Wang, X., and Sheng, G.: An Improved Absorption Ångström Exponent (AAE)-Based Method for Evaluating the Contribution of Light Absorption from Brown Carbon with a High-Time Resolution, Aerosol and Air Quality Research, 19, 15-24, 10.4209/aaqr.2017.12.0566, 2019a.

Zhang, G. H., Peng, L., Lian, X. F., Lin, Q. H., Bi, X. H., Chen, D. H., Li, M., Li, L., Wang, X. M., and Sheng, G. Y.: An Improved Absorption Angstrom Exponent (AAE)-Based Method for Evaluating the Contribution of Light Absorption from Brown Carbon with a High-Time Resolution, Aerosol and Air Quality Research, 19, 15-24, 10.4209/aaqr.2017.12.0566, 2019b.

Zhao, G., Tao, J., Kuang, Y., Shen, C., Yu, Y., and Zhao, C.: Role of black carbon mass size distribution in the direct aerosol radiative forcing, Atmos. Chem. Phys., 19, 13175-13188, 10.5194/acp-19-13175-2019, 2019.

Zhao, G., Yu, Y., Tian, P., Li, J., Guo, S., and Zhao, C.: Evaluation and Correction of the Ambient Particle Spectral Light Absorption Measured Using a Filter-based Aethalometer, Aerosol and Air Quality Research, 20, 1833-1841, 10.4209/aaqr.2019.10.0500, 2020.